JACS
JOURNAL OF THE AMERICAN CHEMICAL SOCIETY
pubs.acs.org/JACS
Article

Organic Photovoltaic Catalyst with Extended Exciton Diffusion for High-Performance Solar Hydrogen Evolution

Yufan Zhu,[▽] Zhenzhen Zhang,[▽] Wenqin Si,[▽] Qianlu Sun,[▽] Guilong Cai, Yawen Li, Yixiao Jia, Xinhui Lu, Weigao Xu, Shiming Zhang,* and Yuze Lin*

Cite This: J. Am. Chem. Soc. 2022, 144, 12747−12755

Read Online

ACCESS | Metrics & More | Article Recommendations | Supporting Information

ABSTRACT: The short exciton diffusion length (L_D) associated with most classical organic photocatalysts (5−10 nm) imposes severe limits on photocatalytic hydrogen evolution efficiency. Here, a photovoltaic molecule (F1) without electron-deficient units at the central building block was designed and synthesized to improve the photoluminescence quantum yield (PLQY). With the enhanced PLQY of 9.3% and a large integral spectral overlap of 3.32×10^{16} nm^4 M^{-1} cm^{-1}, the average L_D of F1 film increases to 20 nm, nearly twice the length of the control photovoltaic molecule (Y6). Then, the single-component organic nanoparticles (SC-NPs) based on F1 show an optimized average hydrogen evolution rate (HER) of 152.60 mmol h^{-1} g^{-1} under AM 1.5G sunlight (100 mW cm^{-2}) illumination for 10 h, which is among the best results for photocatalytic hydrogen evolution.

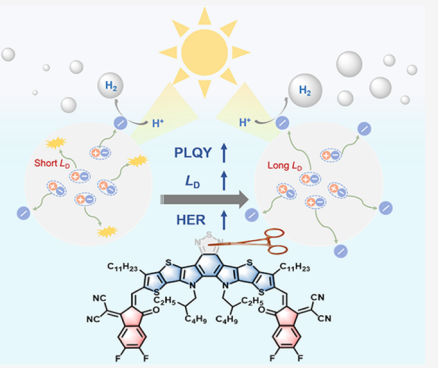

INTRODUCTION

Hydrogen produced through the solar-light-driven splitting of water has been considered the most potential candidate for clean and high-energy-density energy carriers.[1−4] Since the photocatalytic activity of carbon nitride in photocatalytic hydrogen evolution was reported in 2009,[5] a lot of attention has been paid to organic photocatalysts due to their potential advantages in terms of the tunable chemical structure and optical and electronic properties,[6−8] especially broader absorption toward visible and near-infrared (NIR) light, relative to their traditional inorganic counterparts like TiO_2[9] and $SrTiO_3$.[10] Organic semiconductors currently used as photocatalysts for hydrogen evolution mainly included covalent organic frameworks (COFs),[11,12] polymeric carbon nitride,[13,14] and photovoltaic polymer/organic nanoparticles (NPs).[15−17] Among the reported organic photocatalysts, photovoltaic polymer/organic NPs are easily solution-processed, have the most diversified strategies to optimize chemical structure/property, and have achieved the best hydrogen evolution rate (HER) so far.[18]

Excitons governed the optoelectronic functionalities of organic semiconductors because the high exciton binding energies (usually >300 meV)[19,20] prevented the spontaneous dissociation of exciton within organic semiconductors. Thus, exciton diffusion has important implications in organic photocatalytic hydrogen evolution, similar to other optoelectronic applications, such as solar cell devices.[21] Longer exciton diffusion distance ensures that more excitons within semiconductors can reach the interface and dissociate to charge carriers before radiative or nonradiative recombination.[22,23] However, organic semiconductors suffered from very short exciton diffusion length (L_D, 5−10 nm),[24] which limited the improvement of their energy conversion efficiency in light-harvesting applications. In addition to single-component organic NPs (SC-NPs) with a considerable simplification of the optimization process and NP fabrication,[25] polymer/organic bulk heterojunction nanoparticles (BHJ-NPs), in which electron donors and electron acceptors were blended, have been proved to provide more interfaces for exciton dissociation and promote the improvement of photocatalytic hydrogen efficiency,[17,26−30] but still required that exciton efficiently diffused from the pure donor or acceptor domain to donor/acceptor interface, usually the distances of tens nanometers depend on the domain sizes of pure donor/acceptor. Thus, it is still necessary to develop efficient organic photocatalysts with long L_D to boost the improvement in the photocatalytic hydrogen evolution efficiency of photovoltaic polymer/organic NPs, especially for SC-NPs.

Here, we design and synthesize a photovoltaic organic photocatalyst, named F1 (Figure 1), that does not employ the central electron-withdrawing units widely existing in high-performance electron acceptors, such as "thiadiazole" of Y6 (Figure 1).[31] Relative to Y6, F1 exhibits obviously higher

Received: March 24, 2022
Published: July 11, 2022

https://doi.org/10.1021/jacs.2c03161
J. Am. Chem. Soc. 2022, 144, 12747−12755

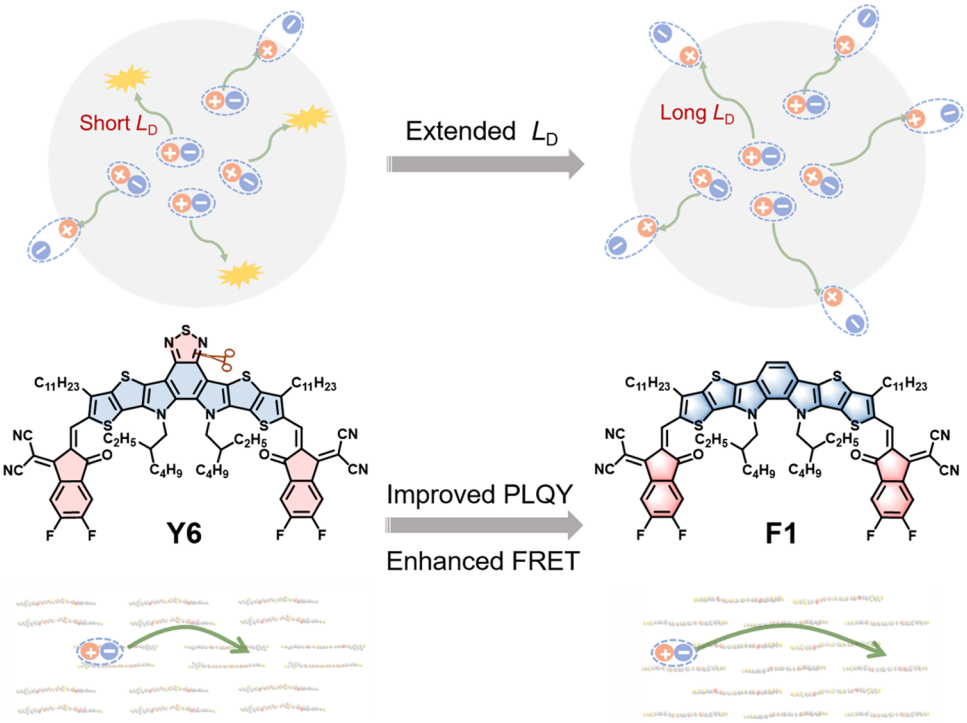

Figure 1. Diagram of motivation. Relative to Y6 with a central electron-deficient unit (thiadiazole), F1 without thiadiazole exhibits higher PLQY and longer L_D. Longer L_D ensures that more excitons within semiconductors can reach the interface and dissociate to charge carriers before recombination. The blue solid spheres represent electrons and the orange solid spheres represent holes. Solid blue and orange spheres surrounded by dashed lines represent excitons. The yellow lightning shapes represent exciton recombination. The thin green arrows represent diffusion. The thick green arrows represent the FRET.

photoluminescence quantum yield (PLQY) of 9.3%, and a larger integral spectral overlap (J) of 3.32×10^{16} nm^4 M^{-1} cm^{-1}, leading to a longer calculated L_D of 20 nm. The average hydrogen evolution rate (HER) for the SC-NPs based on F1 is more than twice that of Y6 under the same test conditions (AM 1.5G, 100 mW cm^{-2} illumination for 10 h). The optimized average HER of F1 NPs reaches 152.60 mmol h^{-1} g^{-1}. To the best of our knowledge, this value of 152.60 mmol h^{-1} g^{-1} is one of the best results for the photocatalytic hydrogen evolution from organic SC-NP photocatalysts,[18,32] even higher than those reported for some BHJ-NPs[17,26−28] and 1−3 orders higher than those reported for some inorganic catalysts.[9,33]

RESULTS AND DISCUSSION

Molecular Design and Synthesis. In an organic semiconductor, exciton diffusion occurs through a series of successive Förster resonant energy transfers (FRETs) between chromophores.[34] FRET is an electrostatic dipole−dipole interaction between chromophores that needs spectral overlap between absorption and emission of chromophores, a short distance between the chromophores, as well as an appropriate orientation of their transition dipoles. The rate of Förster energy transfer (k_F) between two molecules can be quantified as follows[35]

$$k_F = \frac{1}{\tau_0}\left(\frac{R_0}{R}\right)^6 \quad (1)$$

where R is assumed as the average intermolecular distances, τ_0 is the intrinsic exciton lifetime that is not limited by diffusion-limited quenching at defects,[36] and R_0 is the Förster radius[37]

$$R_0^6 = \frac{9k^2\varphi_{PL}J}{128\pi^5 N_A n^4} \quad (2)$$

where k^2 is the dipole−dipole orientation factor (for rigid and randomly oriented dipoles, $k^2 = 0.476$[38]), φ_{PL} is the PLQY, J is the spectral overlap integral between the emission (normalized) and absorption (extinction coefficient of the film) of chromophores, N_A is the Avogadro number, and n is the refractive index.[34] Clearly, improving the PLQY benefits enhance the energy transfer within the organic semiconductor, thereby increasing the L_D.[34,39] Most of the reported high-performance photovoltaic molecules, such as Y6 and its derivatives have an electron-deficient unit at the central building block, such as the "thiadiazole",[31] "triazole",[40] and "pyrazine"[41] units. However, these central electron-deficient groups usually attenuated or quenched the fluorescence of the fluorophore because they could increase the reorganization energy,[42] leading to the increased nonradiative recombination rate.[43,44] Thus, to improve the PLQY and L_D, we designed the F1, which employed a typical acceptor−donor−acceptor (A−D−A) curved molecular structure based on a nitrogen heterocyclic electron-donating core (Figure 1), without the central electron-deficient groups like Y6 and its derivatives. Coincidentally, while our manuscript was under review, Yi et al. theoretically simulated the electronic structures of Y6 and F1[45] and confirmed that F1 exhibited smaller reorganization energy for the $S_0 \leftrightarrow S_1$ state than Y6 (106 meV for F1; 116 meV for Y6). The smaller reorganization energy is beneficial to the enhanced PLQY,[43,44] decreased Stokes shift,[39] and faster exciton diffusion.[45] This theoretical simulation results support the fact that our design is reasonable for improving the PLQY and L_D by removing the central electron-deficient group.

https://doi.org/10.1021/jacs.2c03161
J. Am. Chem. Soc. 2022, 144, 12747−12755

Scheme 1. Typical Synthetic Routes of the Central Fused Rings for Y6 and Its Derivatives. The Possible Methods to Synthesize 1,4-Dibromo-2,3-dinitrobenzene, One Critical Intermediate for Constructing F1 Assuming to Adopt the Similar Route of Y6. The Method We Used Here to Synthesize the Central Fused Ring for F1[a]

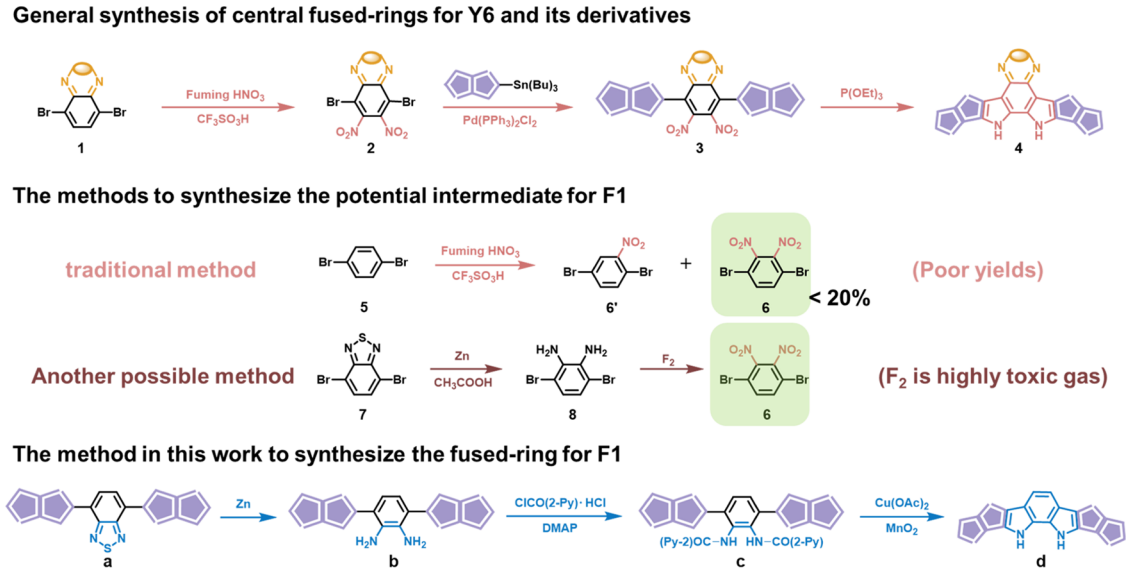

[a]The purple rings represent thieno[3,2-*b*]thiophene and its derivatives, and the yellow ellipses represent sulfur atom, selenium atom, ethylene, and other derivatives. DMAP is the abbreviation of 4-dimethylaminopyridine.

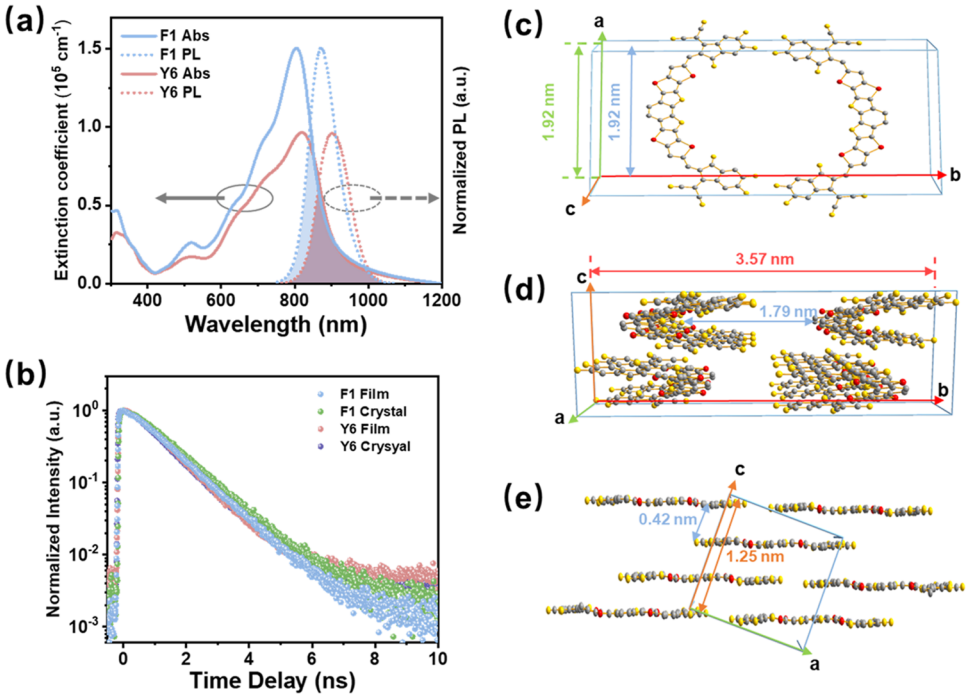

Figure 2. (a) Absorption coefficient and normalized PL of F1 film and Y6 film. (b) Time-resolved photoluminescence of F1 film, F1 crystal, Y6 film, and Y6 crystal. (c–e) Unit cells of F1 viewed from different directions. The green, red, and orange arrows represent the lengths of *a*-, *b*-, and *c*-axes, respectively. The blue arrows represent the distance between adjacent molecules on the corresponding axis.

The core synthesis steps of F1 are different from those of traditional Y6 and its derivatives. As shown in Scheme 1, for Y6 and its derivatives, pyrrole-bridging rings (**4**) are obtained by Cadogan ring-closure reaction between the compound (**3**) and triethyl phosphate.[46] However, the primary product of nitrification of 1,4-dibromobenzene (**5**) is mono-nitrated 1,4-bibromo-2-nitrobenzene (**6′**) rather than 1,4-dibromo-2,3-dinitrobenzene (**6**).[47] Moreover, in another potential option, the oxidation of 3,6-dibromobenzene-1,2-diamine (**8**) to nitro compounds (**6**) requires the participation of the highly toxic gas (F_2).[48] Therefore, pyrrole-bridging rings (**d**) cannot be readily obtained according to the traditional methods mentioned above because the corresponding nitro compound (**6**) is difficult to be synthesized. Inspired by the synthesis of *N*,*S*-based bisacene (bisthienodiindole) in 75% yield reported by Miura et al.,[49] we distinctively synthesize pyrrole-bridging

https://doi.org/10.1021/jacs.2c03161
J. Am. Chem. Soc. 2022, 144, 12747−12755

Table 1. Parameters for Calculating L_D Using the FRET Theory

organic materials	PLQY (%)	J (nm^4 M^{-1} cm^{-1})	n	R_0 (nm)	τ_0 (ns)	ave. R (nm)	ave. D (cm^2 s^{-1})	τ_f (ns)	L_D (nm)
F1	9.3	3.32×10^{16}	3.21	3.3	1.11	0.84	3.8×10^{-2}	1.06	20
Y6	5.6	2.19×10^{16}	3.07	2.9	1.00	0.89	1.6×10^{-2}	0.97	12

rings (**d**) from compound (**c**) through a Cu-catalyzed intramolecular C−H/N−H amination strategy without the use of highly toxic reagents, which provides another synthetic method for pyrrole-bridging rings. The compound (**c**) is obtained using compound (**a**) as the starting material, which then undergoes a reduction reaction and condensation reaction (Scheme 1). The rest of the synthesis steps for F1 are similar to those of the reactions used in the synthesis of Y6 and its derivatives, such as alkylation reaction, nucleophilic reaction, and Knoevenagel condensation reaction (Scheme S1 and Spectral Chart of NMR).

Light Absorption. The strong solar-light-harvesting ability of photocatalyst is one of the preconditions for the high performance solar hydrogen evolution. The maximum extinction coefficient of the F1 chloroform solution (10^{-6} M) is 2.3×10^5 M^{-1} cm^{-1}, which is higher than that of Y6 (1.71×10^5 M^{-1} cm^{-1}).[31] The absorption onset of F1 film extends to 901 nm compared to its solution (Figure S1). Moreover, F1 film exhibits a higher maximum extinction coefficient (1.5×10^5 cm^{-1} at 805 nm, Figure 2a) than that of Y6 film (9.7×10^4 cm^{-1} at 820 nm), and the enhanced absorption of F1 is beneficial to the increased photocatalytic performance, especially in a relatively low concentration of catalyst in which the incident light is not totally absorbed.

Morphology. In addition to the molecular electronic structure, molecular ordering and crystalline properties are also important to exciton diffusion. The grazing incidence wide-angle X-ray scattering (GIWAXS) measurement is used to study the morphological structures of the F1 film (Figure S2). The F1 film presents an out-of-plane (OOP) $\pi-\pi$ peak at q = 1.74 $Å^{-1}$ (d = 3.61 Å) with the crystalline coherence length (CCL) of 24.8 Å. Furthermore, F1 shows an in-plane (IP) lamellar peak (q = 0.41 $Å^{-1}$, d = 15.32 Å, CCL = 70.7 Å), indicating that F1 shows regular molecular ordering. These CCL values of F1 in both OOP and IP directions are larger than those of the corresponding peaks of Y6 (d = 15.70 Å, CCL = 37.7 Å, IP; d = 3.63 Å, CCL = 18.2 Å, OOP).[50] Compared to Y6, the enhanced CCLs of F1 imply that the F1 film has lesser grain boundaries, which decrease the non-radiative recombination and benefit the improved PLQY and contribute to extended L_D.[51]

Exciton Diffusion. Photocatalytic reactions occurring at organic photocatalysts are initiated by charge carriers (electron and hole) generation following the photoinduced excitons diffuse to the surfaces of catalysts. Only those excitons generated at a distance shorter than L_D are effective in dissociating to free charge carriers. The R_0 value, one critical parameter for quantifying L_D, should first be calculated according to eq 2. The PLQY of the F1 film (9.3%) we measured here is higher than that of the Y6 film (5.6%), supporting the fact that PLQY can be improved by removing the central electron-withdrawing units in Y6 and its derivatives. As shown in Figure 2a, compared with the Y6 film (stokes shift: 1136 cm^{-1}; J: 2.19×10^{16} nm^4 M^{-1} cm^{-1}), the F1 film showed a higher extinction coefficient discussed above and smaller stokes shift (928 cm^{-1}), leading to a larger J (3.32×10^{16} nm^4 M^{-1} cm^{-1}). Then, n is obtained by taking the average refractive index of the medium in the wavelength range at which spectral overlap is significant.[52] Although the n of F1 (3.21) is slightly larger than that of Y6 (3.07, Figure S3), R_0 of F1 (3.3 nm) is still obviously larger than that of Y6 (2.9 nm) due to the higher PLQY and larger J.

Furthermore, L_D was calculated by the FRET theory, which is a relatively easy method to estimate the diffusion coefficient since no fitting or modeling software is needed.[52,53] Although FRET theory is an indirect method, the L_D obtained from FRET theory is in good agreement with other directly measured L_D values.[52,54] The exciton diffusion coefficient (D) can be estimated using Smoluchowski−Einstein theory of random walks and connects to the rate of k_F expressed as[55]

$$D = AR^2k_F = A\frac{R_0^6}{\tau_0 R^4} \tag{3}$$

where A is a constant. We use the photoluminescence lifetime of a single crystal to calculate the τ_0 by assuming that there are no exciton quenching defects in the single crystal. As shown in Figure 2b, the τ_0 of F1 and Y6 are 1.11 and 1.00 ns, respectively. Here, we evaluate the approximation of the R from the closest intermolecular distance in a single crystal using the same method reported by Nguyen et al.[52] The minimum value of R is obtained from the shortest intermolecular distances in the single crystal. Therefore, the single-crystal structure of F1 is investigated by single-crystal X-ray diffraction (XRD). The F1 single crystal has a monoclinic crystal system and the $C2/c$ space group. The details can be viewed from the crystallographic information file (CIF, Supporting Information, Table S1). As shown in Figure 2c−e, the intermolecular distances of the a-, b-, and c-axes are 1.92, 1.79, and 0.42 nm, respectively. Thus, the minimum value of R for F1 is 0.42 nm. The maximum value of R is obtained by assuming that molecules are positioned in cubic lattice[52] using eq 4[56]

$$R = \frac{1}{\sqrt[3]{\frac{\rho}{M_W}N_A}} \tag{4}$$

where ρ is the theoretical density obtained from XRD data and M_W is the molecular weight. The maximum value of R for F1 is 1.26 nm, with ρ of 1.15 g cm^{-3} and M_W of 1393 g mol^{-1}. The maximum (1.29 nm) and minimum (0.48 nm) values of R for Y6[57] were calculated using the same method as F1. The D is calculated following eq 3 with R_0, τ_0, and R. The calculated average D of F1 is 3.8×10^{-2} cm^2 s^{-1} according to the average R value (0.84 nm). In contrast, the calculated average D of Y6 is 1.6×10^{-2} cm^2 s^{-1} compared with 0.89 nm of the average R.

Then, L_D is equal to[58]

$$L_D = \sqrt{D\tau_f} = \sqrt{A\frac{\tau_f}{\tau_0}\frac{R_0^3}{R^2}} \tag{5}$$

where τ_f is the photoluminescence lifetime in a sample. The values of τ_f of the F1 and Y6 thin films are 1.06 ns and 0.97 ns, respectively (Figure 2b). According to eq 5, the calculated average L_D of the F1 thin film is 20 nm, which is nearly twice

https://doi.org/10.1021/jacs.2c03161
J. Am. Chem. Soc. 2022, 144, 12747−12755

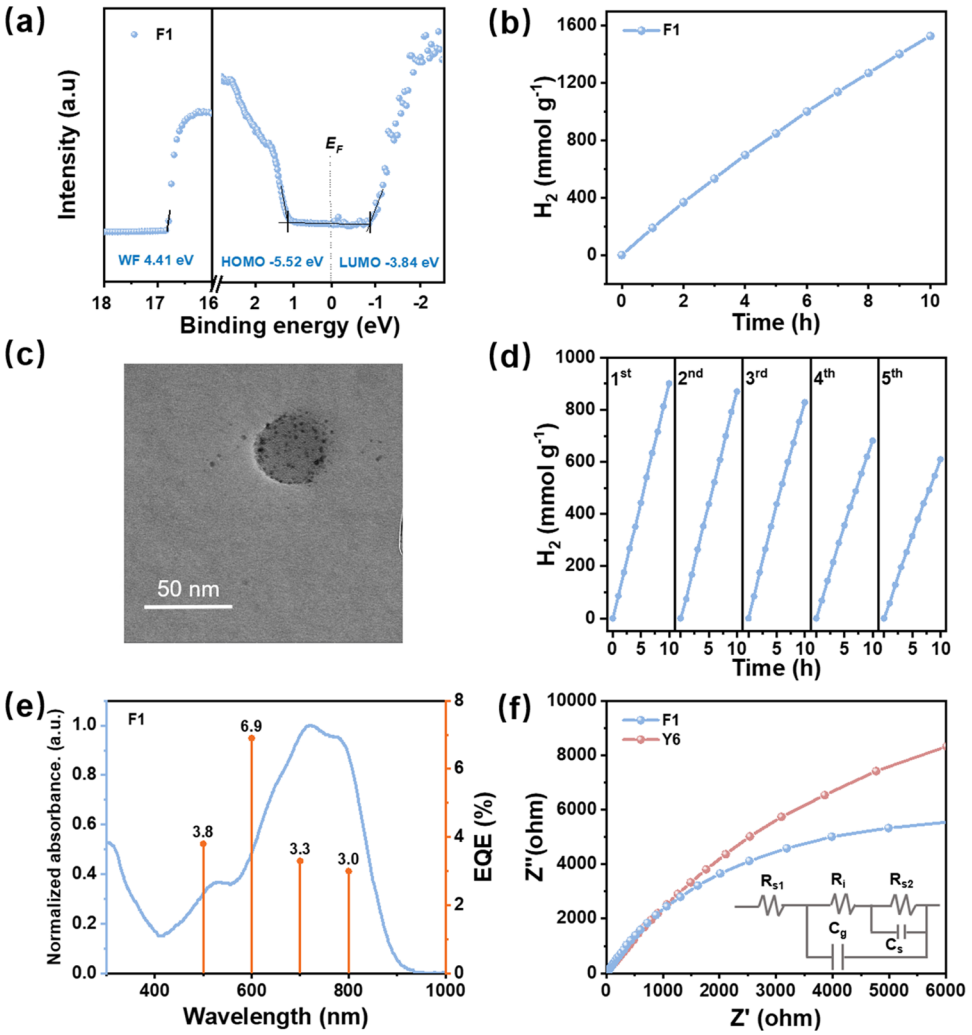

Figure 3. (a) UPS and LEIPS spectra of F1, with respect to the Fermi energy level (E_F) at 0 eV (work function (WF) values are labeled). (b) H_2 evolution vs time of the optimized F1 NPs (0.4 wt % TEBS and 33 wt % Pt loading) at the concentration of 15.63 μg mL^{-1}, under AM 1.5G (100 mW cm^{-2}). (c) Cryo-TEM image of F1 NPs after the deposition of the Pt cocatalyst. The black dots represent Pt. (d) Recycling experiments of hydrogen evolution of F1 NPs (6.67 μg mL^{-1}) under AM 1.5G (100 mW cm^{-2}). For recycling experiments, the equivalent amount of ascorbic acid is added after the end of every cycle, according to the consumption of ascorbic acid. (e) EQE and absorption spectrum of F1 NP photocatalysts. (f) Electrochemical impedance spectroscopy Nyquist plot of F1 NPs and Y6 NPs. The inset is the equivalent circuit. R_{s1} is the series resistance, R_i is the internal resistance, R_{s2} is the surface resistance, C_g is the geometry capacitance, and C_s is the surface capacitance.

that of the Y6 film (12 nm) calculated by the same method. All of the detailed parameters of the L_D calculation are listed in Table 1. It should be noted here there are usually some differences in the results obtained by measuring L_D with different methods for the same material in the literature.[23] The L_D (12 nm) we obtained for the Y6 thin film here is very close to the L_D calculated by the exciton−exciton annihilation method reported by Wei et al. (10.6 nm).[59]

Energy Level. Apart from the strong photon-capturing capability and long L_D, the character of the energy levels of photocatalyst with respect to the reduction and oxidation levels are also critical for solar HER.[60] Ultraviolet photoelectron spectroscopy (UPS) is used to calculate the highest occupied molecular orbital (HOMO) and low-energy inverse photoemission spectroscopy (LEIPS) is used to calculate the lowest unoccupied molecular orbital (LUMO) of F1[26] (Figure 3a). The LUMO energy levels of F1 (−3.84 eV) are higher than those of Y6 (−4.03 eV),[61] indicating that F1 possesses sufficient thermodynamic driving force to reduce proton (−4.32 eV)[26] and more efficient charge separation relative to Y6.[60] Moreover, the HOMO energy level of F1 (−5.52 eV) is lower than the oxidation potential (−4.72 eV)[26] of the ascorbic acid, which means that the hole of F1 can be efficiently extracted by ascorbic acid.

Hydrogen Evolution. F1 is expected to have potential in photocatalytic hydrogen evolution on account of the strong light absorption capability, long L_D, and appropriate energy levels. Then, we optimize the hydrogen evolution performance of single-component F1 NPs by varying sacrificial agents and controlling weight ratios of sodium 2-(3-thienyl) ethyloxybutylsulfonate (TEBS) and Pt-loading ratios (Figures S4−S6), where TEBS and Pt were stabilizing surfactant[17] and cocatalyst. Unlike ascorbic acid, there was no detectable hydrogen production when using weakly basic triethanolamine and neutral ethylene glycol as sacrificial agents (Figure S4), which did not provide enough driving force for proton reduction here.[62] The average HER of F1 NPs (6.67 μg mL^{-1}) is 88.69 mmol h^{-1} g^{-1} (with a maximum HER of 115.93 mmol h^{-1} g^{-1}) at an optimized 0.4 wt % TEBS and 33 wt % Pt ratio loadings for 10 h under AM 1.5G (100 mW cm^{-2}), while an

https://doi.org/10.1021/jacs.2c03161
J. Am. Chem. Soc. 2022, 144, 12747−12755

average HER of 123.15 mmol h^{-1} g^{-1} under 400−800 nm visible-light illumination (100 mW cm^{-2}; Figure S7). In addition, we further measure the hydrogen evolution of F1 NPs at different concentrations with the optimized 0.4 wt % TEBS and 33 wt % Pt ratio loadings (Figure S8 and Table S2) under AM 1.5G (100 mW cm^{-2}). F1 NPs exhibit the highest hydrogen production of 216.6 μmol for 10 h at the concentration of 33.74 μg mL^{-1} and the highest average HER of 152.60 mmol h^{-1} g^{-1} at the concentration of 15.63 μg mL^{-1} (Figure 3b). These average HER values are among the best results for the photocatalytic hydrogen evolution from organic photocatalyst SC-NPs,[18,32] even higher than those reported for some BHJ-NPs,[17,26−28] and 1−3 orders better than those reported for some inorganic catalysts.[9,33] The dynamic light scattering (DLS) results show the size distribution of F1 NPs with different TEBS weight ratios (0.3−0.75 wt %; Figure S9), which reveals that the average nanoparticle diameter is around 44−71 nm, which is dependent on the TEBS content. The radius of these NPs (about 22−35 nm) is close to the L_D of F1, which ensures that most of the excitons can diffuse to the interface to dissociate to charge carriers. The average F1 NP diameter is 46.4 nm with an optimized TEBS weight ratio of 0.4 wt %. Then, Cryo-transmission electron microscopy (Cryo-TEM) is used to investigate the morphologies of F1 NPs with optimized TEBS weight ratios and Pt ratio loadings (Figures 3c and S10), which shows that the average diameter of F1 NPs is 44.2 ± 14.8 nm. From the typical Cryo-TEM photograph of F1 NP (Figure 3c), Pt can be clearly observed to be dispersed on the surface of F1 NPs with a size of several nanometers, which facilitates the transfer of electrons from F1 NPs to H^+.[63] Then, the photocatalytic cycling stability of F1 NPs is investigated (Figure 3d). The F1 NPs exhibit good stability after three cycles, and the HER retains 77 and 68% of the value of the first cycle at the end of the fourth cycle and fifth cycle, respectively. As shown in Figure S11, the NPs aggregated with the increase in the number of test cycles, which contributed to the decrease in catalytic activity. Moreover, we used Cryo-TEM and matrix-assisted laser desorption/ionization-time of flight mass spectrometry (MALDI-TOF MS) to check the variations in the morphology and molecular structure of the F1 NPs after the fifth cycle of the stability test. As shown in Figure S12, F1 NPs have an average diameter of 68.3 ± 27.2 nm, which is significantly larger than that of the initial F1 NPs. The obvious aggregation phenomenon of F1 NPs is consistent with that observed by DLS. As shown in Figure S13, MALDI-TOF MS results show that there are a few weak fragment peaks with a lower molecular weight than that (m/z: 1393.30) of F1, indicating a slight decomposition of the photocatalyst after the stability test. The initial zeta-potential of F1 NPs with 0.4 wt % TEBS, which showed an optimized HER, is −16.5 mV, indicating that these NPs have negative charges on their surfaces with fair stability of the suspension,[64] and there is some room to improve the stability by increasing the absolute value of the zeta-potential of NPs.

As a comparison, we first evaluate the catalytic performance of Y6 SC-NPs under the same condition with optimized TEBS and Pt ratios for F1 (0.4 wt % TEBS and 33 wt % Pt ratio loadings). As shown in Figure S7, the average HER of Y6 (6.67 μg mL^{-1}) is 39.18 mmol h^{-1} g^{-1}, which is less than half that of F1 NPs (88.69 mmol h^{-1} g^{-1}) under AM 1.5G irradiation at 100 mW cm^{-2} for 10 h. Moreover, with a decreased Pt ratio loading (30 wt %), the HER of Y6 NPs drops to 24.14 mmol h^{-1} g^{-1} (Figure S14a), while the HER of F1 is still as high as 80.27 mmol h^{-1} g^{-1} (Figure S6). When the concentration is increased from 6.67 to 33.74 μg mL^{-1}, in which the absorption of catalyst is almost saturated and should not limit the photocatalytic performance, Y6 NPs exhibit a hydrogen production of 103.7 μmol for 10 h (Figure S14b), which is also lower than that of F1 NPs (216.6 μmol) at the same concentration. The DLS results show that the average size of Y6 NPs (80.4 nm, Figure S15) is larger than that of F1 NPs (46.4 nm) fabricated under the same conditions. To minimize the influence of the NP size on the catalytic performance, we tune the size of NPs by changing the weight ratios of TEBS (0.4−2 wt %). When the weight ratio of TEBS is increased to 2 wt.%, the average size of Y6 NPs decreases to 55.1 nm (Figure S15), comparable to the size of optimized F1 NPs (Figure S9). However, these Y6 NPs only show an average HER of 22.94 mmol h^{-1} g^{-1} (Figure S16) under AM 1.5G (100 mW cm^{-2}) for 10 h. These results indicate that F1 NPs show better photocatalytic hydrogen evolution performance than Y6 NPs, which can mainly be attributed to the extended exciton diffusion of F1.

Furthermore, the external quantum efficiency (EQE) values of F1 SC-NPs are greater than or equal to 3% and can reach 6.9% at a wavelength of 600 nm (Figure 3e). The EQE of F1 SC-NPs, measured in absorption saturation, is much higher than that of Y6 SC-NPs (<2.5%; Figure S17), which should be mainly attributed to a longer L_D of F1. To better understand the photocatalytic process of H_2 generation, the efficiency of charge extraction was studied by electrochemical impedance spectroscopy. Compared with Y6 NPs, the F1 NPs display a smaller semicircle (Figure 3f), indicating that the efficiency of charge separation and transfer of F1 is higher than that of Y6 NPs,[65,66] leading to a higher HER of F1.

CONCLUSIONS

In summary, we developed an organic photovoltaic photocatalyst (F1) with a high PLQY (9.3%) by employing an A−D−A curved molecular structure through a new synthetic method for pyrrole-bridging rings. Combined with the large J, F1 exhibited extended average L_D of 20 nm, which was nearly twice as long as that of Y6. The SC-NPs based on F1 showed an optimized average HER of 152.60 mmol h^{-1} g^{-1} under one sun (AM 1.5G, 100 mW cm^{-2}) illumination for 10 h. To the best of our knowledge, this average HER was among the best results for photocatalytic hydrogen evolution from organic photocatalysts and was much better than those of inorganic catalysts. The work revealed that optimizing electronic properties by regulating the molecular structure was promising for developing photovoltaic materials with a long L_D and promoting improvements in photocatalytic hydrogen evolution from organic semiconductors. This strategy should be extended to some other related fields, like organic solar cells and photodetectors.

ASSOCIATED CONTENT

Supporting Information

The Supporting Information is available free of charge at https://pubs.acs.org/doi/10.1021/jacs.2c03161.

Experimental Section: materials, synthesis, and characterization; Scheme S1, Tables S1−S2, Figures S1−S19, and crystallographic information of single-crystal structure of F1 (2160777) (PDF)

https://doi.org/10.1021/jacs.2c03161
J. Am. Chem. Soc. 2022, 144, 12747−12755

Accession Codes

CCDC 2160777 contains the supplementary crystallographic data for this paper. These data can be obtained free of charge via www.ccdc.cam.ac.uk/data_request/cif, or by emailing data_request@ccdc.cam.ac.uk, or by contacting The Cambridge Crystallographic Data Centre, 12 Union Road, Cambridge CB2 1EZ, UK; fax: +44 1223 336033.

AUTHOR INFORMATION

Corresponding Authors

Yuze Lin − *Beijing National Laboratory for Molecular Sciences, CAS Key Laboratory of Organic Solids, Institute of Chemistry, Chinese Academy of Sciences, Beijing 100190, China; University of Chinese Academy of Sciences, Beijing 100049, China;* orcid.org/0000-0002-0325-3842; Email: linyz@iccas.ac.cn

Shiming Zhang − *Key Laboratory of Flexible Electronics (KLOFE) & Institute of Advanced Materials (IAM), Jiangsu National Synergetic Innovation, Center for Advanced Materials (SICAM), Nanjing Tech University, Nanjing 211816 Jiangsu, China;* orcid.org/0000-0002-7062-6661; Email: iamsmzhang@njtech.edu.cn

Authors

Yufan Zhu − *Beijing National Laboratory for Molecular Sciences, CAS Key Laboratory of Organic Solids, Institute of Chemistry, Chinese Academy of Sciences, Beijing 100190, China; Key Laboratory of Flexible Electronics (KLOFE) & Institute of Advanced Materials (IAM), Jiangsu National Synergetic Innovation, Center for Advanced Materials (SICAM), Nanjing Tech University, Nanjing 211816 Jiangsu, China*

Zhenzhen Zhang − *Beijing National Laboratory for Molecular Sciences, CAS Key Laboratory of Organic Solids, Institute of Chemistry, Chinese Academy of Sciences, Beijing 100190, China; University of Chinese Academy of Sciences, Beijing 100049, China*

Wenqin Si − *Beijing National Laboratory for Molecular Sciences, CAS Key Laboratory of Organic Solids, Institute of Chemistry, Chinese Academy of Sciences, Beijing 100190, China; University of Chinese Academy of Sciences, Beijing 100049, China*

Qianlu Sun − *Key Laboratory of Mesoscopic Chemistry, School of Chemistry and Chemical Engineering, Nanjing University, Nanjing 210023, China*

Guilong Cai − *Department of Physics, The Chinese University of Hong Kong, Hong Kong 999077, China;* orcid.org/0000-0001-9924-1362

Yawen Li − *Beijing National Laboratory for Molecular Sciences, CAS Key Laboratory of Organic Solids, Institute of Chemistry, Chinese Academy of Sciences, Beijing 100190, China; University of Chinese Academy of Sciences, Beijing 100049, China*

Yixiao Jia − *Beijing National Laboratory for Molecular Sciences, CAS Key Laboratory of Organic Solids, Institute of Chemistry, Chinese Academy of Sciences, Beijing 100190, China; Key Laboratory of Flexible Electronics (KLOFE) & Institute of Advanced Materials (IAM), Jiangsu National Synergetic Innovation, Center for Advanced Materials (SICAM), Nanjing Tech University, Nanjing 211816 Jiangsu, China*

Xinhui Lu − *Department of Physics, The Chinese University of Hong Kong, Hong Kong 999077, China;* orcid.org/0000-0002-1908-3294

Weigao Xu − *Key Laboratory of Mesoscopic Chemistry, School of Chemistry and Chemical Engineering, Nanjing University, Nanjing 210023, China;* orcid.org/0000-0002-3014-756X

Complete contact information is available at: https://pubs.acs.org/10.1021/jacs.2c03161

Author Contributions

[▽]Y.Z., Z.Z., W.S., and Q.S. contributed equally to this work.

Notes

The authors declare no competing financial interest.

ACKNOWLEDGMENTS

The authors thank the National Natural Science Foundation of China (52173189) for financial support. They also thank Prof. Yeteng Zhong for helping with the measurement of the refractive index, Prof. Yilin Wang, Prof. Fengting Lv, and Prof. Shu Wang for helping with the DLS measurement, and Kaiang Liu for the Cryo-TEM measurement.

REFERENCES

(1) Fujishima, A.; Honda, K. Electrochemical Photolysis of Water at a Semiconductor Electrode. *Nature* **1972**, *238*, 37−38.

(2) Sivula, K.; Roel, V. Semiconducting Materials for Photoelectrochemical Energy Conversion. *Nat. Rev. Mater.* **2016**, *1*, No. 15010.

(3) Chen, S.; Takata, T.; Domen, K. Particulate Photocatalysts for Overall Water Splitting. *Nat. Rev. Mater.* **2017**, *2*, No. 17050.

(4) Nishiyama, H.; Yamada, T.; Nakabayashi, M.; Maehara, Y.; Yamaguchi, M.; Kuromiya, Y.; Nagatsuma, Y.; Tokudome, H.; Akiyama, S.; Watanabe, T.; Narushima, R.; Okunaka, S.; Shibata, N.; Takata, T.; Hisatomi, T.; Domen, K. Photocatalytic Solar Hydrogen Production from Water on a 100-m^2 Scale. *Nature* **2021**, *598*, 304−307.

(5) Wang, X.; Maeda, K.; Thomas, A.; Takanabe, K.; Xin, G.; Carlsson, J. M.; Domen, K.; Antonietti, M. A Metal-free Polymeric Photocatalyst for Hydrogen Production from Water under Visible Light. *Nat. Mater.* **2009**, *8*, 76−80.

(6) Wang, L.; Fernandez-Teran, R.; Zhang, L.; Fernandes, D. L.; Tian, L.; Chen, H.; Tian, H. Organic Polymer Dots as Photocatalysts for Visible Light-driven Hydrogen Generation. *Angew. Chem., Int. Ed.* **2016**, *55*, 1−6.

(7) Sprick, R. S.; Jiang, J. X.; Bonillo, B.; Ren, S.; Ratvijitvech, T.; Guiglion, P.; Zwijnenburg, M. A.; Adams, D. J.; Cooper, A. I. Tunable Organic Photocatalysts for Visible-light-driven Hydrogen Evolution. *J. Am. Chem. Soc.* **2015**, *137*, 3265−3270.

(8) Shanmugam, S.; Boyer, C. Organic Photocatalysts for Cleaner Polymer Synthesis. *Science* **2016**, *352*, 1053−1054.

(9) Lee, B. H.; Park, S.; Kim, M.; Sinha, A. K.; Lee, S. C.; Jung, E.; Chang, W. J.; Lee, K. S.; Kim, J. H.; Cho, S. P.; Kim, H.; Nam, K. T.; Hyeon, T. Reversible and Cooperative Photoactivation of Single-atom Cu/TiO_2 Photocatalysts. *Nat. Mater.* **2019**, *18*, 620−626.

(10) Goto, Y.; Hisatomi, T.; Wang, Q.; Higashi, T.; Ishikiriyama, K.; Maeda, T.; Sakata, Y.; Okunaka, S.; Tokudome, H.; Katayama, M.; Akiyama, S.; Nishiyama, H.; Inoue, Y.; Takewaki, T.; Setoyama, T.; Minegishi, T.; Takata, T.; Yamada, T.; Domen, K. A Particulate Photocatalyst Water-splitting Panel for Large-scale Solar Hydrogen Generation. *Joule* **2018**, *2*, 509−520.

(11) Banerjee, T.; Lotsch, B. V. The Wetter the Better. *Nat. Chem.* **2018**, *10*, 1175−1177.

(12) Wang, X.; Chen, L.; Chong, S. Y.; Little, M. A.; Wu, Y.; Zhu, W. H.; Clowes, R.; Yan, Y.; Zwijnenburg, M. A.; Sprick, R. S.; Cooper, A. I. Sulfone-containing Covalent Organic Frameworks for Photo-

catalytic Hydrogen Evolution from Water. *Nat. Chem.* **2018**, *10*, 1180−1189.
(13) Meng, N.; Ren, J.; Liu, Y.; Huang, Y.; Petit, T.; Zhang, B. Engineering Oxygen-containing and Amino Groups into Two-Dimensional Atomically-thin Porous Polymeric Carbon Nitrogen for Enhanced Photocatalytic Hydrogen Production. *Energy Environ. Sci.* **2018**, *11*, 566−571.
(14) Wang, Y.; Bayazit, M. K.; Moniz, S. J. A.; Ruan, Q.; Lau, C. C.; Martsinovich, N.; Tang, J. Linker-controlled Polymeric Photocatalyst for Highly Efficient Hydrogen Evolution from Water. *Energy Environ. Sci.* **2017**, *10*, 1643−1651.
(15) Dai, C.; Liu, B. Conjugated Polymers for Visible-light-driven Photocatalysis. *Energy Environ. Sci.* **2020**, *13*, 24−52.
(16) Zhang, H.; Liu, G.; Shi, L.; Liu, H.; Wang, T.; Ye, J. Engineering Coordination Polymers for Photocatalysis. *Nano Energy* **2016**, *22*, 149−168.
(17) Kosco, J.; Bidwell, M.; Cha, H.; Martin, T.; Howells, C. T.; Sachs, M.; Anjum, D. H.; Gonzalez Lopez, S.; Zou, L.; Wadsworth, A.; Zhang, W.; Zhang, L.; Tellam, J.; Sougrat, R.; Laquai, F.; DeLongchamp, D. M.; Durrant, J. R.; McCulloch, I. Enhanced Photocatalytic Hydrogen Evolution from Organic Semiconductor Heterojunction Nanoparticles. *Nat. Mater.* **2020**, *19*, 559−565.
(18) Liu, Y.; Wu, J.; Wang, F. Dibenzothiophene-S,S-dioxide-containing Conjugated Polymer with Hydrogen Evolution Rate up to 147 mmol g^{-1} h^{-1}. *Appl. Catal., B* **2022**, *307*, No. 121144.
(19) Zhu, L.; Zhang, J.; Guo, Y.; Yang, C.; Yi, Y.; Wei, Z. Small Exciton Binding Energies Enabling Direct Charge Photogeneration Towards Low-driving-force Organic Solar Cells. *Angew. Chem., Int. Ed.* **2021**, *60*, 15348−15353.
(20) Scholes, G. D.; Rumbles, G. Excitons in Nanoscale Systems. *Nat. Mater.* **2006**, *5*, 683−696.
(21) Holmes, R. J. Enhancing Energy Transport in Conjugated Polymers. *Science* **2018**, *360*, 854−855.
(22) Mikhnenko, O. V.; Azimi, H.; Scharber, M.; Morana, M.; Blom, P. W. M.; Loi, M. A. Exciton Diffusion Length in Narrow Bandgap Polymers. *Energy Environ. Sci.* **2012**, *5*, 6960−6965.
(23) Sajjad, M. T.; Ruseckas, A.; Samuel, I. D. W. Enhancing Exciton Diffusion Length Provides New Opportunities for Organic Photovoltaics. *Matter* **2020**, *3*, 341−354.
(24) Mikhnenko, O. V.; Kuik, M.; Lin, J.; van der Kaap, N.; Nguyen, T. Q.; Blom, P. W. Trap-limited Exciton Diffusion in Organic Semiconductors. *Adv. Mater.* **2014**, *26*, 1912−1917.
(25) Roncali, J. Single Material Solar Cells: the Next Frontier for Organic Photovoltaics? *Adv. Energy Mater.* **2011**, *1*, 147−160.
(26) Zhang, Z.; Si, W.; Wu, B.; Wang, W.; Li, Y.; Ma, W.; Lin, Y. Two-Dimensional Polycyclic Photovoltaic Molecule with Low Trap Density for High-Performance Photocatalytic Hydrogen Evolution. *Angew. Chem., Int. Ed.* **2022**, *134*, No. e202114234.
(27) Liu, A.; Gedda, L.; Axelsson, M.; Pavliuk, M.; Edwards, K.; Hammarstrom, L.; Tian, H. Panchromatic Ternary Polymer Dots Involving Sub-picosecond Energy and Charge Transfer for Efficient and Stable Photocatalytic Hydrogen Evolution. *J. Am. Chem. Soc.* **2021**, *143*, 2875−2885.
(28) Kosco, J.; Gonzalez-Carrero, S.; Howells, C. T.; Zhang, W.; Moser, M.; Sheelamanthula, R.; Zhao, L.; Willner, B.; Hidalgo, T. C.; Faber, H.; Purushothaman, B.; Sachs, M.; Cha, H.; Sougrat, R.; Anthopoulos, T. D.; Inal, S.; Durrant, J. R.; McCulloch, I. Oligoethylene Glycol Side Chains Increase Charge Generation in Organic Semiconductor Nanoparticles for Enhanced Photocatalytic Hydrogen Evolution. *Adv. Mater.* **2022**, *34*, No. 2105007.
(29) Kosco, J.; Gonzalez-Carrero, S.; Howells, C. T.; Fei, T.; Dong, Y.; Sougrat, R.; Harrison, G. T.; Firdaus, Y.; Sheelamanthula, R.; Purushothaman, B.; Moruzzi, F.; Xu, W.; Zhao, L.; Basu, A.; De Wolf, S.; Anthopoulos, T. D.; Durrant, J. R.; McCulloch, I. Generation of Long-lived Charges in Organic Semiconductor Heterojunction Nanoparticles for Efficient Photocatalytic Hydrogen Evolution. *Nat. Energy* **2022**, *7*, 340−351.
(30) Yang, H.; Li, X.; Sprick, R. S.; Cooper, A. I. Conjugated Polymer Donor-molecular Acceptor Nanohybrids for Photocatalytic Hydrogen Evolution. *Chem. Commun.* **2020**, *56*, 6790−6793.
(31) Yuan, J.; Zhang, Y.; Zhou, L.; Zhang, G.; Yip, H.-L.; Lau, T.-K.; Lu, X.; Zhu, C.; Peng, H.; Johnson, P. A.; Leclerc, M.; Cao, Y.; Ulanski, J.; Li, Y.; Zou, Y. Single-junction Organic Solar Cell with over 15% Efficiency Using Fused-ring Acceptor with Electron-deficient Core. *Joule* **2019**, *3*, 1140−1151.
(32) Shu, C.; Han, C.; Yang, X.; Zhang, C.; Chen, Y.; Ren, S.; Wang, F.; Huang, F.; Jiang, J. X. Boosting the Photocatalytic Hydrogen Evolution Activity for D-π-A Conjugated Microporous Polymers by Statistical Copolymerization. *Adv. Mater.* **2021**, *33*, No. 2008498.
(33) Park, S.; Chang, W. J.; Lee, C. W.; Park, S.; Ahn, H.-Y.; Nam, K. T. Photocatalytic Hydrogen Generation from Hydriodic Acid Using Methylammonium Lead Iodide in Dynamic Equilibrium with Aqueous Solution. *Nat. Energy* **2017**, *2*, No. 16185.
(34) Menke, S. M.; Luhman, W. A.; Holmes, R. J. Tailored Exciton Diffusion in Organic Photovoltaic Cells for Enhanced Power Conversion Efficiency. *Nat. Mater.* **2013**, *12*, 152−157.
(35) Förster, T. 10th Spiers Memorial Lecture. Transfer Mechanisms of Electronic Excitation. *Discuss. Faraday Soc.* **1959**, *27*, 7−17.
(36) Mikhnenko, O. V.; Blom, P. W. M.; Nguyen, T.-Q. Exciton Diffusion in Organic Semiconductors. *Energy Environ. Sci.* **2015**, *8*, 1867−1888.
(37) Förster, T. Zwischenmolekulare Energiewanderung und Fluoreszenz. *Ann. Phys.* **1948**, *437*, 55−75.
(38) Steinberg, I. Z. Long-Range Nonradiative Transfer of Electronic Excitation Energy in Proteins and Polypeptides. *Annu. Rev. Biochem.* **1971**, *40*, 83−114.
(39) Firdaus, Y.; Le Corre, V. M.; Karuthedath, S.; Liu, W.; Markina, A.; Huang, W.; Chattopadhyay, S.; Nahid, M. M.; Nugraha, M. I.; Lin, Y.; Seitkhan, A.; Basu, A.; Zhang, W.; McCulloch, I.; Ade, H.; Labram, J.; Laquai, F.; Andrienko, D.; Koster, L. J. A.; Anthopoulos, T. D. Long-range Exciton Diffusion in Molecular Non-fullerene Acceptors. *Nat. Commun.* **2020**, *11*, No. 5220.
(40) Liu, S.; Yuan, J.; Deng, W.; Luo, M.; Xie, Y.; Liang, Q.; Zou, Y.; He, Z.; Wu, H.; Cao, Y. High-efficiency Organic Solar Cells with Low Non-radiative Recombination Loss and Low Energetic Disorder. *Nat. Photonics* **2020**, *14*, 300−305.
(41) Zhou, Z.; Liu, W.; Zhou, G.; Zhang, M.; Qian, D.; Zhang, J.; Chen, S.; Xu, S.; Yang, C.; Gao, F.; Zhu, H.; Liu, F.; Zhu, X. Subtle Molecular Tailoring Induces Significant Morphology Optimization Enabling over 16% Efficiency Organic Solar Cells with Efficient Charge Generation. *Adv. Mater.* **2020**, *32*, No. 1906324.
(42) Chai, S.; Wen, S.-H.; Huang, J.-D.; Han, K.-L. Density Functional Theory Study on Electron and Hole Transport Properties of Organic Pentacene Derivatives with Electron-withdrawing Substituent. *J. Comput. Chem.* **2011**, *32*, 3218−3225.
(43) Xie, Y.; Du, N.; Yu, S.; Zhang, L.; Yang, M. Unraveling the Structure-Dependent Radiative and Nonradiative Decays in $(CdSe)_{13}$ Clusters through First-principles Calculations. *J. Phys. Chem. C* **2019**, *123*, 30714−30722.
(44) Wei, Y.-C.; Wang, S. F.; Hu, Y.; Liao, L.-S.; Chen, D.-G.; Chang, K.-H.; Wang, C-W.; Liu, S.-H.; Chan, W.-H.; Liao, J.-L.; Hung, W.-Y.; Wang, T.-H.; Chen, P.-T.; Hsu, H.-F.; Chi, Y.; Chou, P.-T. Overcoming the Energy Gap Law in Near-infrared OLEDs by Exciton-Vibration Decoupling. *Nat. Photonics* **2020**, *14*, 570−577.
(45) Guo, Y.; Han, G.; Yi, Y. The Intrinsic Role of the Fusion Mode and Electron-Deficient Core in Fused-Ring Electron Acceptors for Organic Photovoltaics. *Angew. Chem., Int. Ed.* **2022**, No. e202205975.
(46) Wei, Q.; Liu, W.; Leclerc, M.; Yuan, J.; Chen, H.; Zou, Y. A-DA′D-A Non-fullerene Acceptors for High-performance Organic Solar Cells. *Sci. China: Chem.* **2020**, *63*, 1352−1366.
(47) Błaszczyk, A.; Chadim, M.; von Hänisch, C.; Mayor, M. Synthesis of Macrocyclic Molecular Rods as Potential Electronic Devices. *Eur. J. Org. Chem.* **2006**, *2006*, 3809−3825.
(48) Dirk, S. M.; M, E. T.; Henderson, J. C.; Tour, J. M. Oxidation of Electron-Deficient Anilines by HOF. A Route to Nitro-containing

https://doi.org/10.1021/jacs.2c03161
J. Am. Chem. Soc. 2022, 144, 12747−12755

Compounds for Molecular Electronic Devices. *Org. Lett.* **2000**, *2*, 3405−3406.
(49) Takamatsu, K.; Hirano, K.; Satoh, T.; Miura, M. Synthesis of Carbazoles by Copper-catalyzed Intramolecular C-H/N-H Coupling. *Org. Lett.* **2014**, *16*, 2892−2895.
(50) Zhang, Z.; Li, Y.; Cai, G.; Zhang, Y.; Lu, X.; Lin, Y. Selenium Heterocyclic Electron Acceptor with Small Urbach Energy for As-Cast High-Performance Organic Solar Cells. *J. Am. Chem. Soc.* **2020**, *142*, 18741−18745.
(51) Lunt, R. R.; Benziger, J. B.; Forrest, S. R. Relationship Between Crystalline Order and Exciton Diffusion Length in Molecular Organic Semiconductors. *Adv. Mater.* **2010**, *22*, 1233−1236.
(52) Lin, J. D. A.; Mikhnenko, O. V.; Chen, J.; Masri, Z.; Ruseckas, A.; Mikhailovsky, A.; Raab, R. P.; Liu, J.; Blom, P. W. M.; Loi, M. A.; García-Cervera, C. J.; Samuel, I. D. W.; Nguyen, T.-Q. Systematic Study of Exciton Diffusion Length in Organic Semiconductors by Six Experimental Methods. *Mater. Horiz.* **2014**, *1*, 280−285.
(53) Menke, S. M.; Holmes, R. J. Exciton Diffusion in Organic Photovoltaic Cells. *Energy Environ. Sci.* **2014**, *7*, 499−512.
(54) Lunt, R. R.; Giebink, N. C.; Belak, A. A.; Benziger, J. B.; Forrest, S. R. Exciton Diffusion Lengths of Organic Semiconductor Thin Films Measured by Spectrally Resolved Photoluminescence Quenching. *J. Appl. Phys.* **2009**, *105*, No. 053711.
(55) Powell, R. C.; Soos, Z. G. Singlet Exciton Energy Transfer in Organic Solids. *J. Lumin.* **1975**, *11*, 1−45.
(56) Li, Z.; Lin, J. D. A.; Phan, H.; Sharenko, A.; Proctor, C. M.; Zalar, P.; Chen, Z.; Facchetti, A.; Nguyen, T.-Q. Competitive Absorption and Inefficient Exciton Harvesting: Lessons Learned from Bulk Heterojunction Organic Photovoltaics Utilizing the Polymer Acceptor P(NDI2OD-T2). *Adv. Funct. Mater.* **2014**, *24*, 6989−6998.
(57) Lin, F.; Jiang, K.; Kaminsky, W.; Zhu, Z.; Jen, A. K. A Non-fullerene Acceptor with Enhanced Intermolecular π-Core Interaction for High-Performance Organic Solar Cells. *J. Am. Chem. Soc.* **2020**, *142*, 15246−15251.
(58) Chandrabose, S.; Chen, K.; Barker, A. J.; Sutton, J. J.; Prasad, S. K. K.; Zhu, J.; Zhou, J.; Gordon, K. C.; Xie, Z.; Zhan, X.; Hodgkiss, J. M. High Exciton Diffusion Coefficients in Fused Ring Electron Acceptor Films. *J. Am. Chem. Soc.* **2019**, *141*, 6922−6929.
(59) Shi, Y.; Chang, Y.; Lu, K.; Chen, Z.; Zhang, J.; Yan, Y.; Qiu, D.; Liu, Y.; Adil, M. A.; Ma, W.; Hao, X.; Zhu, L.; Wei, Z. Small Reorganization Energy Acceptors Enable Low Energy Losses in Non-fullerene Organic Solar Cells. *Nat. Commun.* **2022**, *13*, No. 3256.
(60) Kosco, J.; Moruzzi, F.; Willner, B.; McCulloch, I. Photocatalysts Based on Organic Semiconductors with Tunable Energy Levels for Solar Fuel Applications. *Adv. Energy Mater.* **2020**, *10*, No. 2001935.
(61) Li, T.; Wang, K.; Cai, G.; Li, Y.; Liu, H.; Jia, Y.; Zhang, Z.; Lu, X.; Yang, Y.; Lin, Y. Asymmetric Glycolated Substitution for Enhanced Permittivity and Ecocompatibility of High-Performance Photovoltaic Electron Acceptor. *JACS Au* **2021**, *1*, 1733−1742.
(62) Han, C.; Dong, P.; Tang, H.; Zheng, P.; Zhang, C.; Wang, F.; Huang, F.; Jiang, J. X. Realizing High Hydrogen Evolution Activity under Visible Light Using Narrow Band Gap Organic Photocatalysts. *Chem. Sci.* **2021**, *12*, 1796−1802.
(63) McKone, J. R.; Marinescu, S. C.; Brunschwig, B. S.; Winkler, J. R.; Gray, H. B. Earth-abundant Hydrogen Evolution Electrocatalysts. *Chem. Sci.* **2014**, *5*, 865−878.
(64) Sen, S.; Dasgupta, S.; DasGupta, S. Does Surface Chirality of Gold Nanoparticles Affect Fibrillation of HSA? *J. Phys. Chem. C* **2017**, *121*, 18935−18946.
(65) Zhou, P.; Chen, H.; Chao, Y.; Zhang, Q.; Zhang, W.; Lv, F.; Gu, L.; Zhao, Q.; Wang, N.; Wang, J.; Guo, S. Single-atom Pt-I_3 Sites on All-inorganic Cs_2SnI_6 Perovskite for Efficient Photocatalytic Hydrogen Production. *Nat. Commun.* **2021**, *12*, No. 4412.
(66) Yue, X.; Yi, S.; Wang, R.; Zhang, Z.; Qiu, S. Well-controlled $SrTiO_3$@Mo_2C Core-shell Nanofiber Photocatalyst: Boosted Photogenerated Charge Carriers Transportation and Enhanced Catalytic Performance for Water Reduction. *Nano Energy* **2018**, *47*, 463−473.

https://doi.org/10.1021/jacs.2c03161
J. Am. Chem. Soc. 2022, 144, 12747−12755